

A high-order wideband direct solver for electromagnetic scattering from bodies of revolution

Charles L. Epstein*, Leslie Greengard† and Michael O’Neil ‡

September 5, 2022

Abstract

The generalized Debye source representation of time-harmonic electromagnetic fields yields well-conditioned second-kind integral equations for, among others, the problems of scattering from perfect electric conductors and dielectric bodies. Furthermore, these representations, and resulting integral equations, are fully stable in the static limit as $\omega \rightarrow 0$ in multiply connected geometries. In this paper, we present the first high-order accurate solver based on this representation for bodies of revolution, and compare with existing schemes based on classical representations and integral equations. The resulting solver uses a Nyström discretization of a generating curve, with spectral-integral methods for applying and inverting surface differentials. The accuracy and speed of the solver are demonstrated in several numerical examples.

Keywords: Maxwell’s equations, second-kind integral equations, magnetic field integral equation, generalized Debye sources, perfect electric conductor, body of revolution

1 Introduction

In isotropic homogenous media, the time-harmonic Maxwell’s equations governing the propagation of electric and magnetic fields are given by [35]

$$\begin{aligned} \nabla \times \mathbf{E} &= i\omega\mu\mathbf{H}, & \nabla \times \mathbf{H} &= \mathbf{J} - i\epsilon\omega\mathbf{E}, \\ \nabla \cdot \mathbf{E} &= \frac{\rho}{\epsilon}, & \nabla \cdot \mathbf{H} &= 0, \end{aligned} \tag{1.1}$$

where \mathbf{E} and \mathbf{H} are the electric and magnetic fields, respectively, and ω is the angular frequency. The electric charge is denoted by ρ and the electric current by \mathbf{J} . The electric permittivity and magnetic permeability are given by ϵ and μ , respectively, and assumed to be piecewise constant in all that follows. It will be useful to define the wavenumber k as $k = \omega\sqrt{\epsilon\mu}$, and we assume that $\Im(k) \geq 0$. The implicit time dependence of $e^{-i\omega t}$ on \mathbf{E} , \mathbf{H} has been suppressed.

*Mathematics Department, University of Pennsylvania, Philadelphia, PA. Email: cle@math.upenn.edu. Research supported in part by NSF awards DMS-150739 and DMS-1205851.

†Courant Institute, New York University, New York, NY and Flatiron Institute, New York, NY. Email: greengard@cims.nyu.edu. Research supported in part by the by the Office of the Assistant Secretary of Defense for Research and Engineering and AFOSR under NSSEFF Program award FA9550-10-1-0180.

‡Courant Institute, New York University, New York, NY. Email: oneil@cims.nyu.edu. Research supported in part by the by the Office of the Assistant Secretary of Defense for Research and Engineering and AFOSR under NSSEFF Program award FA9550-10-1-0180 and the Office of Naval Research under awards N00014-17-1-2059 and N00014-17-1-2451.

Maxwell's equations in the above form provide a surprisingly accurate approximation to physical phenomena, and therefore their accurate numerical solution is of the utmost importance in several fields, such as radio-frequency component modeling [27], meta-material simulation [20], and radar cross-section characterizations [44]. This list is certainly not exhaustive. Several computational methods for the solution to (1.1) are used in practice, including finite differences [42] (mostly used in the time-domain), finite elements and spectral methods [28, 31], and integral equations [32]. Finite difference and finite element methods are particularly useful when the material parameters vary in space, and especially when the fields are anisotropic. However, recent advances in integral equation methods for variable coefficient PDEs are likely to compete with existing finite difference and finite element methods [2].

On the other hand, when applicable – namely in complex geometries with piecewise constant material parameters – boundary integral equation methods are the preferred solution as they often outperform all other methods in terms of computational cost and scalability. Two standard problems in electromagnetics – scattering from perfect electric conductors and dielectric bodies – fit exactly these assumptions [26]. Boundary integral equation methods are particularly useful in these scattering problems, where unbounded geometries are the norm and integral representations explicitly construct physically meaningful solutions. While high-order accurate methods in arbitrary geometries in three dimensions are still lacking, there are several important applications of Maxwell's equations in scattering from bodies of revolution [18, 24, 29, 30]. In this setup, it is possible to build very high-order accurate quasi-optimal solvers using separation of variables and the Fast Fourier Transform (FFT) which scale roughly as $O(N^{3/2})$, where N is the number of unknowns needed to fully discretize the body's surface in three dimensions (i.e. $\sim \sqrt{N}$ in each direction).

Despite the applicability of these separation of variables integral equation-based solvers to bodies of revolution, wideband solvers have yet to be implemented that are applicable in both the genus-one case and in the low-frequency regime (as $\omega \rightarrow 0$). This is mainly due to two reasons: (1) constructing high-order accurate Nyström methods (including quadrature) for the so-called modal Green's functions [9] is somewhat technical, and (2) existing integral equation methods suffered from ill-conditioning due to *dense-mesh breakdown* and *topological breakdown* [10, 11, 13] in the static limit. The algorithm of this paper, based on the recent generalized Debye source formulations of Maxwell fields [11, 13] overcomes both of these obstacles. The past few years has seen several developments in electrostatic and acoustic scattering from bodies of revolution [23, 43]. Only the work of [29] fully treated the vector-valued integral equation case, but used the method of fundamental solutions [3, 15] instead of the direct boundary integral discretization. In this work, we provide a more thorough discussion of the calculations required in the vector case as it is more complicated than the scalar case. Classically, scattering from bodies of revolution was very popular in the electrical engineering community. We do not seek to review the entire literature, as it is too broad, but rather point out relevant previous work when discussing particular topics: quadrature, kernel evaluation, and integral equation conditioning.

The paper is organized as follows: Section 2 introduces the generalized Debye source formulation of Maxwell fields, as well provides the relevant boundary value problems for scattering from perfect conductors and dielectric bodies. Section 3 derives the necessary formulations required for separating vector-valued functions in cylindrical coordinates on surfaces of revolution. Section 4 describes a high-order Nyström-type solver for electromagnetic scattering. This includes a discussion of quadrature, kernel evaluation, and surface differential application. We provide several numerical example demonstrating our algorithm in Section 5 and then discuss extensions and drawbacks of the scheme in Section 6.

2 Generalized Debye sources

Classically, most integral equations for electromagnetic scattering problems have been derived from with the standard Lorenz gauge representation of the electric and magnetic fields using a scalar potential φ and vector potential \mathbf{A} [35]:

$$\begin{aligned}\mathbf{E} &= i\omega\mathbf{A} - \nabla\varphi \\ \mathbf{H} &= \frac{1}{\mu}\nabla \times \mathbf{A}.\end{aligned}\tag{2.1}$$

In the Lorenz gauge $\nabla \cdot \mathbf{A} = \varphi$, and in particular,

$$\mathbf{A}(\mathbf{x}) = \int \frac{e^{ik|\mathbf{x}-\mathbf{x}'|}}{4\pi|\mathbf{x}-\mathbf{x}'|} \mathbf{J}(\mathbf{x}') d\mathbf{x}', \quad \varphi(\mathbf{x}) = \int \frac{e^{ik|\mathbf{x}-\mathbf{x}'|}}{4\pi|\mathbf{x}-\mathbf{x}'|} \frac{\nabla \cdot \mathbf{J}}{i\omega} d\mathbf{x}'.\tag{2.2}$$

In the case of the perfect electric conductor, using these representations immediately yields the Electric Field Integral Equation (EFIE), Magnetic Field Integral Equation (MFIE), and by taking linear combinations of these, the Combined Field Integral Equation (CFIE) [7]. Unless additional preconditioners are used [8], the EFIE and CFIE suffer from what is known as *low-frequency dense-mesh breakdown* due to the division by ω in the scalar potential term. This can be circumvented by explicitly invoking the consistency condition $\nabla \cdot \mathbf{J} = i\omega\rho$ (which is implied by Maxwell's equations) to define the scalar potential as $\varphi = \mathcal{S}_k\rho$. Additional boundary conditions must be added because of the addition of an extra unknown, but this is straightforward. See [38, 40, 41] for various *charge-current formulations* of scattering problems. However, as discussed in the introduction, another form of low-frequency breakdown occurs in Maxwell's equations: *topological low-frequency breakdown* [11]. This form of breakdown is characterized by ill-conditioned, or mathematically non-invertible, integral equations as $\omega \rightarrow 0$. The generalized Debye source representation of Maxwell's fields is one of only two representations which overcomes both dense-mesh and topological low-frequency breakdown [11, 13]. (The other formulation being the Decoupled Potential Integral Equation (DPIE) [41].) In current and charge free regions, after suitable scaling the time-harmonic Maxwell equations (1.1) can be rewritten as

$$\begin{aligned}\nabla \times \mathbf{E} &= ik\mathbf{H}, & \nabla \times \mathbf{H} &= -ik\mathbf{E}, \\ \nabla \cdot \mathbf{E} &= 0, & \nabla \cdot \mathbf{H} &= 0,\end{aligned}\tag{2.3}$$

where, as before, $k = \sqrt{\epsilon\mu\omega}$. The generalized Debye source representation is a full potential/anti-potential, non-physical representation given by:

$$\begin{aligned}\mathbf{E} &= ik\mathbf{A} - \nabla\varphi - \nabla \times \mathbf{Q}, \\ \mathbf{H} &= ik\mathbf{Q} - \nabla\psi + \nabla \times \mathbf{A},\end{aligned}\tag{2.4}$$

where the potentials are given by

$$\begin{aligned}\mathbf{A} &= \mathcal{S}_k\mathbf{J}, & \varphi &= \mathcal{S}_k\rho, \\ \mathbf{Q} &= \mathcal{S}_k\mathbf{K}, & \psi &= \mathcal{S}_k\sigma.\end{aligned}\tag{2.5}$$

Here, in a slight abuse of notation, \mathbf{J} and ρ are non-physical variables instead of electric current and charge, as in (1.1). In order for Maxwell's equations to be satisfied in a source-free region, the

potentials must satisfy $\nabla \cdot \mathbf{A} = ik\varphi$ and $\nabla \cdot \mathbf{Q} = ik\psi$. This means that the currents and charges must satisfy the following consistency conditions:

$$\nabla_\Gamma \cdot \mathbf{J} = ik\rho, \quad \nabla_\Gamma \cdot \mathbf{K} = ik\sigma, \quad (2.6)$$

where Γ is the boundary of, for example, some perfectly conducting object. While it appears as though \mathbf{J} , \mathbf{K} , ρ , and σ are all unknowns coupled through the consistency conditions, depending on the particular boundary conditions \mathbf{J} and \mathbf{K} are *constructed* from ρ and σ such that the consistency conditions are automatically met. The sources ρ , σ are required to be mean-zero [11], and are referred to as *generalized Debye sources*. The currents \mathbf{J} and \mathbf{K} can then be specified in their Hodge decomposition along Γ :

$$\begin{aligned} \mathbf{J} &= \nabla_\Gamma \alpha_J + \mathbf{n} \times \nabla_\Gamma \beta_J + \mathbf{J}_H, \\ \mathbf{K} &= \nabla_\Gamma \alpha_K + \mathbf{n} \times \nabla_\Gamma \beta_K + \mathbf{K}_H, \end{aligned} \quad (2.7)$$

where α_ℓ and β_ℓ linear in ρ and σ and chosen to meet the consistency conditions. Here, \mathbf{J}_H , \mathbf{K}_H are harmonic vector fields along Γ , that is to say that

$$\nabla_\Gamma \cdot \mathbf{J}_H = 0, \quad \nabla_\Gamma \cdot \mathbf{n} \times \mathbf{J}_H = 0, \quad (2.8)$$

and similarly for \mathbf{K}_H . The dimension of the linear space of harmonic vector fields is $2g$, where g is the genus of (smooth) boundary Γ . In the following, to be explicit we will write

$$\mathbf{J}_H = \sum_{j=1}^{2g} a_j \mathbf{h}_j, \quad \mathbf{K}_H = \sum_{j=1}^{2g} b_j \mathbf{h}_j, \quad (2.9)$$

where the \mathbf{h}_j form a basis for the harmonic vector fields. It is the coefficients a_j , b_j that must be determined based on boundary data. Expression (2.7) is an explicit splitting of \mathbf{J} and \mathbf{K} into their divergence-free, curl-free, and harmonic components along Γ . For boundary-value problems in multiply-connected geometries, in addition to constraints on the values of \mathbf{E} , \mathbf{H} along the surface, the projection of \mathbf{J}_H and \mathbf{K}_H onto the space of harmonic vector fields needs to be fixed. This projection is easily determined by the inclusion of $2g$ separate line integrals of \mathbf{E} , \mathbf{H} along loops contained in Γ which enclose *interior and exterior holes* – that is to say, these loops C_1, \dots, C_{2g} must span the space of first homology groups in $\mathbb{R}^3 \setminus \Omega$ and Ω . This class of extra conditions can take the form:

$$\int_{C_j} \mathbf{E} \cdot d\mathbf{l} = f_j, \quad (2.10)$$

for $j = 1, \dots, 2g$ and some set of constants f_j . See Figure 1 for a plot of a possible set of relevant loops C_j in the genus 1 case.

Unlike various combined-field representations for electromagnetic fields which use the physical variables electric current and charge (which must meet the consistency conditions), representations based on non-physical generalized Debye sources *automatically* satisfy Maxwell's equations by construction. This property is very important in several applications which are not so-called *scattering problems* [14].

2.1 The perfect electric conductor

Along the surface Γ of a perfect electric conductor (PEC) Ω , we have the following physical relationships between the electromagnetic fields and electric current and charge:

$$\begin{aligned} \mathbf{n} \times \mathbf{H}^{\text{tot}} &= \mathbf{J}, & \mathbf{n} \cdot \mathbf{H}^{\text{tot}} &= 0, \\ \mathbf{n} \times \mathbf{E}^{\text{tot}} &= \mathbf{0}, & \mathbf{n} \cdot \mathbf{E}^{\text{tot}} &= \rho. \end{aligned} \quad (2.11)$$

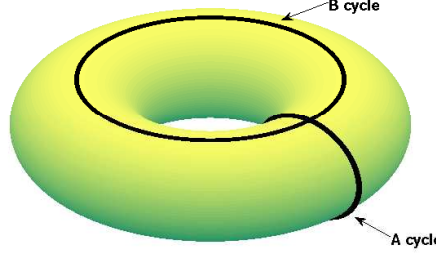


Figure 1: Loops spanning the interior and exterior homologies of a genus 1 surface.

In scattering problems, often the total field \mathbf{E}^{tot} , \mathbf{H}^{tot} is split into two terms: a scattered and an incoming field. We have:

$$\begin{aligned}\mathbf{E}^{\text{tot}} &= \mathbf{E} + \mathbf{E}^{\text{in}}, \\ \mathbf{H}^{\text{tot}} &= \mathbf{H} + \mathbf{H}^{\text{in}}.\end{aligned}\quad (2.12)$$

The field \mathbf{E}^{in} , \mathbf{H}^{in} is known, and used as boundary data in the formulation of the scattering problem. In the case of scattering from a PEC, the current-like vector fields \mathbf{J} and \mathbf{K} in the generalized Debye source representation can be constructed as [11]:

$$\begin{aligned}\mathbf{J} &= ik \left(\nabla_{\Gamma} \Delta_{\Gamma}^{-1} \rho - \mathbf{n} \times \nabla_{\Gamma} \Delta_{\Gamma}^{-1} \sigma \right) + \mathbf{J}_H, \\ \mathbf{K} &= \mathbf{n} \times \mathbf{J},\end{aligned}\quad (2.13)$$

where ∇_{Γ} denotes the surface gradient along Γ and Δ_{Γ}^{-1} denotes the inverse of the Laplace-Beltrami operator along Γ restricted to mean-zero functions. Restricted to mean-zero functions, this operator is uniquely invertible. Using this construction for \mathbf{J} and \mathbf{K} , and enforcing the (preconditioned) [32] homogeneous boundary conditions

$$\begin{aligned}\mathcal{S}_0 \nabla_{\Gamma} \cdot \mathbf{E}^{\text{tot}} &= 0, & \text{on } \Gamma, \\ \mathbf{n} \cdot \mathbf{H}^{\text{tot}} &= 0, & \text{on } \Gamma, \\ \int_{C_j} \mathbf{E}^{\text{tot}} \cdot d\mathbf{l} &= 0, & \text{for } j = 1, \dots, 2g\end{aligned}\quad (2.14)$$

yields a second-kind integral equation for ρ , σ , and \mathbf{J}_H which is uniquely invertible for all values of k with non-negative imaginary part [11]. Here, \mathcal{S}_0 , the zero-frequency single-layer potential operator. The system in (2.14) can be written more explicitly as:

$$\begin{aligned}\frac{1}{4} \rho + \mathcal{K}_E[\rho, \sigma, a_j] &= -\mathcal{S}_0 \nabla_{\Gamma} \cdot \mathbf{E}^{\text{in}}, & \text{on } \Gamma, \\ \frac{1}{2} \sigma + \mathcal{K}_H[\rho, \sigma, a_j] &= -\mathbf{n} \cdot \mathbf{H}^{\text{in}}, & \text{on } \Gamma, \\ \int_{C_j} \mathbf{E}^{\text{tot}} \cdot d\mathbf{l} &= 0, & \text{for } j = 1, \dots, 2g,\end{aligned}\quad (2.15)$$

with the operators \mathcal{K}_E and \mathcal{K}_H given by

$$\begin{aligned}\mathcal{K}_E[\rho, \sigma, a_j] &= ik \mathcal{S}_0 \nabla_{\Gamma} \cdot \mathcal{S}_k \mathbf{J} - \mathcal{S}_0 \Delta_{\Gamma} \mathcal{S}_k \rho - \mathcal{S}_0 \nabla_{\Gamma} \cdot \nabla \times \mathcal{S}_k \mathbf{K}, \\ \mathcal{K}_H[\rho, \sigma, a_j] &= ik \mathbf{n} \cdot \mathcal{S}_k \mathbf{K} - \mathcal{S}'_k \sigma + \mathbf{n} \cdot \nabla \times \mathcal{S}_k \mathbf{J},\end{aligned}\quad (2.16)$$

where

$$\mathcal{S}'_k f(\mathbf{x}) = \frac{\partial}{\partial n} \int_{\Gamma} G(\mathbf{x}, \mathbf{x}') f(\mathbf{x}') da(\mathbf{x}') \quad (2.17)$$

with $\partial/\partial n$ denoting differentiation in the direction normal to Γ at \mathbf{x} , and G denoting the Green's function for the Helmholtz equation:

$$G(\mathbf{x}, \mathbf{x}') = \frac{e^{ik|\mathbf{x}-\mathbf{x}'|}}{4\pi|\mathbf{x}-\mathbf{x}'|}. \quad (2.18)$$

The dependence of \mathbf{J} and \mathbf{K} on the variables ρ and σ and the coefficients a_j has been suppressed for convenience. All integral operators above are interpreted in their on-surface principal-value sense. It is worth pointing out that the third terms in \mathcal{K}_E and \mathcal{K}_H are order-zero operators on \mathbf{J} and \mathbf{K} . They are of order minus-one with regard to the variables ρ and σ , as can be seen from the construction of \mathbf{J} and \mathbf{K} .

Remark 1. *The system of integral equations in (2.14) is uniquely invertible with the restriction that ρ, σ (the generalized Debye sources) and the data are all mean-zero functions. Without explicitly enforcing this condition the system is rank-one deficient, as can be seen from the operator $\mathcal{S}_0 \Delta_{\Gamma} \mathcal{S}_k$. In Section 4.5 we discuss how to explicitly add this constraint in numerically as a rank-one update to the system matrix [37].*

We now turn to a description of a separation of variables, FFT-accelerated solver the system (2.15) when Γ is given as a body of revolution.

3 Integral equations on surfaces of revolution

The numerical solution of boundary integral equations along general curved surfaces in three dimensions has been an active area of research in the past several decades, but high-order accurate fast solvers are out of reach mainly due to complications in singular quadrature, mesh generation, etc. However, when the geometry contains rotational symmetry about, say, the z -axis, separation of variables and Fourier decomposition can be used to turn the problem into a sequence of boundary integral equations along a one-dimensional curve, for which many fast and accurate numerical methods exist. We now setup the geometry of our problem, and detail the separation of variables.

3.1 Geometry

In this section we establish the coordinate system along a surface of revolution Γ , as well as derive the form of surface differentials and the Fourier separation of surface integral equations. The scalar case has been well-treated in [23, 43], but the vector-valued case has not received a thorough modern discussion. See Figure 2 through the discussion for a depiction of the setup and relevant coordinate system.

We will denote the usual unit-vector basis in Cartesian coordinates as $\{\mathbf{i}, \mathbf{j}, \mathbf{k}\}$ and the usual unit-vector basis in cylindrical coordinates as $\{\mathbf{r}, \theta, \mathbf{k}\}$:

$$\begin{aligned} \mathbf{r}(\theta) &= \cos \theta \mathbf{i} + \sin \theta \mathbf{j} & \mathbf{i} &= \cos \theta \mathbf{r}(\theta) - \sin \theta \mathbf{\theta}(\theta) \\ \mathbf{\theta}(\theta) &= -\sin \theta \mathbf{i} + \cos \theta \mathbf{j} & \mathbf{j} &= \sin \theta \mathbf{r}(\theta) + \cos \theta \mathbf{\theta}(\theta) \end{aligned} \quad (3.1)$$

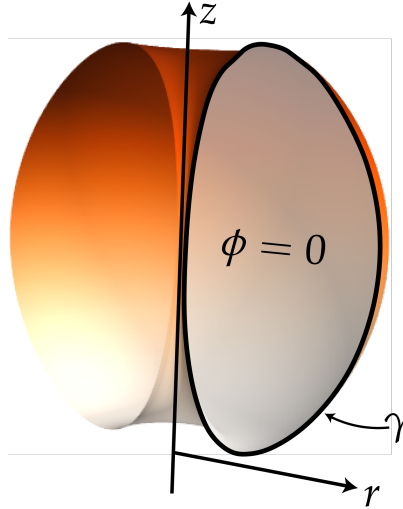


Figure 2: Geometry of a body of revolution.

where we have given formulae for both cylindrical and Cartesian unit vectors in terms of the other. These relationships will be useful in the following sections. The following addition formulae will also be useful:

$$\begin{aligned}\mathbf{r}(\theta - \varphi) &= \cos \varphi \mathbf{r}(\theta) - \sin \varphi \boldsymbol{\theta}(\theta) \\ \boldsymbol{\theta}(\theta - \varphi) &= \sin \varphi \mathbf{r}(\theta) + \cos \varphi \boldsymbol{\theta}(\theta)\end{aligned}\tag{3.2}$$

We will omit the implicit dependence (relative to \mathbf{i} and \mathbf{j}) of \mathbf{r} and $\boldsymbol{\theta}$ on the variable θ from now on, unless it is explicitly required. In order to avoid confusion going forward, *targets* will usually be denoted by \mathbf{x} and *sources* will usually be denoted by \mathbf{x}' . This notation will be consistent with integrating variables as well (integrals will be performed in r' , θ' , and z' variables).

If the boundary Γ of the body of revolution Ω is generated by rotating a curve γ around the z -axis, then points along this curve in \mathbb{R}^2 are given by $\gamma(s) = (r(s), z(s))$, with s denoting arc-length. A local orthonormal basis along Γ (assuming that γ is oriented counter-clockwise) will then be denoted by $\{\boldsymbol{\tau}, \boldsymbol{\theta}, \mathbf{n}\}$ with $\boldsymbol{\theta}$ the usual cylindrical coordinate unit vector and

$$\begin{aligned}\boldsymbol{\tau} &= \frac{dr}{ds} \mathbf{r} + \frac{dz}{ds} \mathbf{k}, \\ \mathbf{n} &= \boldsymbol{\theta} \times \boldsymbol{\tau}.\end{aligned}\tag{3.3}$$

3.2 The scalar function case

Scalar-valued boundary integral equations on surfaces of revolution can be Fourier decomposed straightforwardly, as in [23, 43]. We briefly state the decomposition here, and then thoroughly discuss the vector-valued case.

Along the boundary Γ of a body of revolution, a second-kind integral equation with translation invariant kernel G for the function σ takes the form:

$$\sigma(\mathbf{x}) + \int_{\Gamma} G(\mathbf{x} - \mathbf{x}') \sigma(\mathbf{x}') da(\mathbf{x}') = f(\mathbf{x})\tag{3.4}$$

for $\mathbf{x} \in \Gamma$. In particular, this means that G is rotationally invariant: $G(\mathbf{x} - \mathbf{x}') = G(r, z, r', z', \theta - \theta')$. Expanding the solution σ and right-hand side f in terms of their Fourier series, we have:

$$\sigma(s, \theta) = \sum_{m=-\infty}^{\infty} \sigma_m(s) e^{im\theta}, \quad f(s, \theta) = \sum_{m=-\infty}^{\infty} f_m(s) e^{im\theta}, \quad (3.5)$$

where the Fourier coefficient functions σ_m and f_m are given by

$$\sigma_m(s) = \frac{1}{2\pi} \int_{-\pi}^{\pi} \sigma(s, \theta) e^{-im\theta} d\theta, \quad f_m(s) = \frac{1}{2\pi} \int_{-\pi}^{\pi} f(s, \theta) e^{-im\theta} d\theta. \quad (3.6)$$

Substituting the Fourier representations for σ and f in (3.5) into the integral equation in (3.4) and collecting terms mode-by-mode, we have the following decoupled integral equations along the generating curve γ :

$$\begin{aligned} \sigma_m(s) + \int_{\gamma} \sigma_m(s') \int_{-\pi}^{\pi} G(s, s', \theta - \theta') e^{-im\theta'} r' d\theta' ds' &= f_m(s), \\ \implies \sigma_m(s) + 2\pi \int_{\gamma} G_m(s, s') \sigma_m(s') r' ds' &= f_m(s) \end{aligned} \quad (3.7)$$

for all m , where we denote the Fourier modes of G as G_m :

$$\begin{aligned} G(r, z, r', z', \theta - \theta') &= \sum_{m=-\infty}^{\infty} G_m(r, z, r', z') e^{im(\theta-\theta')} \\ \iff G_m(r, z, r', z') &= \frac{1}{2\pi} \int_{-\pi}^{\pi} G(r, z, r', z', \varphi) e^{-im\varphi} d\varphi. \end{aligned} \quad (3.8)$$

We use the notation $G(s, s', \theta - \theta') = G(\mathbf{x} - \mathbf{x}')$ for when both \mathbf{x} and \mathbf{x}' are located on Γ , and likewise for the Fourier modes G_m . This procedure has reduced the problem of solving a boundary integral equation on a surface embedded in three dimensions to that of solving a sequence of boundary integral equations along curves embedded in two dimensions. Given an efficient method for evaluating the modal Green's functions G_m , performing the synthesis and analysis of σ and f using the Fast Fourier Transform (FFT) [5] yields a very efficient direct solver for the original problem. The efficient evaluation of G_m and related functions for the Helmholtz equation is a long-studied problem, and is discussed in Section 4.2.

We now turn our attention to the analogous problem, that of Fourier decomposing a vector-valued integral equation along a surface of revolution. While the generalized Debye system in (2.15) is defined in terms of scalar-valued unknowns, its discretization requires the application of layer potential operators to vector quantities. Slightly more care is required in this case than in the scalar case.

3.3 The vector-valued case

Similar to the scalar case, a second-kind vector-valued boundary integral equation with translation invariant kernel G is of the form:

$$\mathbf{u}(\mathbf{x}) + \int_{\Gamma} G(\mathbf{x}, \mathbf{x}') \mathbf{u}(\mathbf{x}') da(\mathbf{x}') = \mathbf{f}(\mathbf{x}). \quad (3.9)$$

In the electromagnetic application, frequently both \mathbf{u} , \mathbf{f} are vector fields which are tangential to the boundary Γ due to physical considerations, so we address that case only. (In fact, the vector fields \mathbf{J}

and \mathbf{K} in (2.16) are tangential by construction, and require formulas for the action of layer potentials to their Fourier modes.) Furthermore, the classic MFIE using in scattering problems from PECs explicitly has a vector-valued unknown, physical electric current \mathbf{J} :

$$-\frac{1}{2}\mathbf{J} + \mathbf{n} \times \nabla \times \mathcal{S}_k \mathbf{J} = -\mathbf{n} \times \mathbf{H}^{\text{in}}, \quad \text{on } \Gamma. \quad (3.10)$$

Fully three-dimensional surface vector fields may be encountered in problems in fluid dynamics or elasticity, and many of the following calculations directly extend, albeit with components lying in the direction normal to Γ .

Since Γ is a surface of revolution, the tangential vector fields in (3.9) can be written in terms of their Fourier series, component-wise, with respect to the local basis $\boldsymbol{\tau}, \boldsymbol{\theta}$:

$$\begin{aligned} \mathbf{u}(s, \theta) &= \sum_m \left(u_m^\tau(s) \boldsymbol{\tau} + u_m^\theta(s) \boldsymbol{\theta} \right) e^{im\theta}, \\ \mathbf{f}(s, \theta) &= \sum_m \left(f_m^\tau(s) \boldsymbol{\tau} + f_m^\theta(s) \boldsymbol{\theta} \right) e^{im\theta}. \end{aligned} \quad (3.11)$$

These representations are complete because of the periodicity and regularity of the surface Γ . Since we have that $G = G(r, z, r', z', \theta - \theta') = G(s, s', \theta - \theta')$ for translation invariant kernels along Γ , plugging the Fourier expansion for \mathbf{u} into the integral term in (3.9) we have:

$$\begin{aligned} \int_{\Gamma} G(\mathbf{x} - \mathbf{x}') \mathbf{u}(\mathbf{x}') da(\mathbf{x}') \\ = \int_{\gamma} \int_{-\pi}^{\pi} G(s, s', \theta - \theta') \sum_m \left(u_m^\tau(s') \boldsymbol{\tau}(s', \theta') + u_m^\theta(s') \boldsymbol{\theta}(\theta') \right) e^{im\theta'} r' d\theta' ds', \end{aligned} \quad (3.12)$$

We now calculate the projection of this integral onto the m^{th} Fourier mode with respect to the unit vectors $\mathbf{r}(\theta), \boldsymbol{\theta}(\theta)$. The unit vectors $\mathbf{r}(\theta')$ and $\boldsymbol{\theta}(\theta')$ *cannot* be pulled outside of the integrals, however it is a direct consequence of the addition formulas in equation (3.2) that:

$$\begin{aligned} \int_{-\pi}^{\pi} G(\cdot, \theta - \theta') \mathbf{r}(\theta') e^{im\theta'} d\theta' &= e^{im\theta} \int_{-\pi}^{\pi} G(\cdot, \varphi) \mathbf{r}(\theta - \varphi) e^{-im\varphi} d\varphi \\ &= e^{im\theta} \mathbf{r}(\theta) \int_{-\pi}^{\pi} G(\cdot, \varphi) \cos \varphi e^{-im\varphi} d\varphi \\ &\quad - e^{im\theta} \boldsymbol{\theta}(\theta) \int_{-\pi}^{\pi} G(\cdot, \varphi) \sin \varphi e^{-im\varphi} d\varphi \\ &= e^{im\theta} \left(G_m^{\cos}(\cdot) \mathbf{r}(\theta) - G_m^{\sin}(\cdot) \boldsymbol{\theta}(\theta) \right) \end{aligned} \quad (3.13)$$

where

$$\begin{aligned} G_m^{\cos}(\cdot) &= \int_{-\pi}^{\pi} G(\cdot, \varphi) \cos \varphi e^{-im\varphi} d\varphi, \\ G_m^{\sin}(\cdot) &= \int_{-\pi}^{\pi} G(\cdot, \varphi) \sin \varphi e^{-im\varphi} d\varphi. \end{aligned} \quad (3.14)$$

Likewise, we have that

$$\int_{-\pi}^{\pi} G(\cdot, \theta - \theta') \boldsymbol{\theta}(\theta') e^{im\theta'} d\theta' = e^{im\theta} \left(G_m^{\sin}(\cdot) \mathbf{r}(\theta) + G_m^{\cos}(\cdot) \boldsymbol{\theta}(\theta) \right). \quad (3.15)$$

Recalling that $\boldsymbol{\tau} = \frac{dr}{ds}\boldsymbol{r} + \frac{dz}{ds}\boldsymbol{k}$, the integral equation in (3.9) can be re-written mode by mode for all m , and component-wise as:

$$\begin{aligned}\boldsymbol{r} : \quad & u_m^\tau \frac{dr}{ds} + \int_\gamma \left(G_m^{\cos}(\cdot, s') \frac{dr}{ds'} u_m^\tau + G_m^{\sin}(\cdot, s') u_m^\theta \right) r' ds' = \frac{dr}{ds} f_m^\tau, \\ \boldsymbol{\theta} : \quad & u_m^\theta + \int_\gamma \left(G_m^{\cos}(\cdot, s') u_m^\theta - G_m^{\sin}(\cdot, s') u_m^\tau \frac{dr}{ds'} \right) r' ds' = f_m^\theta, \\ \boldsymbol{k} : \quad & u_m^\tau \frac{dz}{ds} + \int_\gamma G_m(\cdot, s') \frac{dz}{ds'} u_m^\tau r' ds' = \frac{dz}{ds} f_m^\tau.\end{aligned}\quad (3.16)$$

The previous integral equations, while decoupled with respect to Fourier mode m and cylindrical coordinate vector components $\boldsymbol{r}, \boldsymbol{\theta}, \boldsymbol{k}$, are *not* decoupled with respect to the components of \boldsymbol{u}, u_m^τ and u_m^θ . This is due to the action of the integral operator on the local coordinate system, $\boldsymbol{\tau}, \boldsymbol{\theta}, \boldsymbol{n}$. Depending on the exact boundary conditions, linear combinations of the above integral equations may be taken to form an even more coupled, second-kind system (since it is obvious that one could solve for u_m^τ first, and then for u_m^θ). The main point here is to demonstrate that the vector-value case is more involved than the scalar case, and that there are additional kernels that need to be evaluated: G_m^{\cos} and G_m^{\sin} .

The integral equations that we will be discretizing involve the composition of layer potential operators. This case can be handled analogously.

3.4 Surface differentials

The integral equations resulting from the generalized Debye representations make explicit use of the Hodge decomposition of tangential vector fields, and therefore require the application of surface differential operators. In this section we briefly give formulae for these operators along the axisymmetric boundary Γ : the surface gradient ∇_Γ , the surface divergence $\nabla_\Gamma \cdot$, and the surface Laplacian Δ_Γ . Furthermore, the construction of surface currents \boldsymbol{J} and \boldsymbol{K} requires the application of Δ_Γ^{-1} . We provide the formula for Δ_Γ below, and then in Section 4.3 discuss a numerical method for inverting it. In order to somewhat simplify the resulting expressions, we assume that the generating curve γ of the boundary Γ is parameterized by arclength s . Similar formulae with arbitrary parameterizations or curvilinear coordinates can be found in most differential geometry or mathematical physics texts, see for example [16, 32].

Let $f(s, \theta) = g(s) e^{im\theta}$ be a scalar function defined on Γ and $\boldsymbol{F}(s, \theta) = (F_\tau(s) \boldsymbol{\tau} + F_\theta(s) \boldsymbol{\theta}) e^{im\theta}$ be a vector field tangential to Γ . We then have the following three expressions for the surface differentials:

$$\begin{aligned}\nabla_\Gamma f &= \frac{\partial f}{\partial s} \boldsymbol{\tau} + \frac{im}{r} f \boldsymbol{\theta}, \\ \nabla_\Gamma \cdot \boldsymbol{F} &= \frac{\partial F_\tau}{\partial s} + \frac{1}{r} \frac{\partial r}{\partial s} F_\tau + \frac{im}{r} F_\theta, \\ \Delta_\Gamma f &= \frac{\partial^2 f}{\partial s^2} + \frac{1}{r} \frac{\partial r}{\partial s} \frac{\partial f}{\partial s} - \frac{m^2}{r^2} f.\end{aligned}\quad (3.17)$$

The on-surface quantity $\nabla \times \boldsymbol{F}$, where $\nabla \times$ denotes the three-dimensional curl operator, can be computed for the tangential \boldsymbol{F} above by using the standard curl in cylindrical coordinates along with the relationships:

$$\boldsymbol{r} = \frac{dr}{ds} \boldsymbol{\tau} + \frac{dz}{ds} \boldsymbol{n}, \quad \boldsymbol{k} = \frac{dz}{ds} \boldsymbol{\tau} - \frac{dr}{ds} \boldsymbol{n}. \quad (3.18)$$

4 A high-order solver

In this section we detail the various parts of the solver, including the efficient numerical evaluation of the modal Green's functions, application of the surface differentials (and inversion of the surface Laplacian), and stable evaluation of the auxiliary boundary conditions required by the Debye formulation. The resulting linear systems, one for each Fourier mode, are then solved directly using LAPACK's dense LU routines. This part of the computation is not a dominate one, so no large effort was made to accelerate it. First, we describe the Nyström discretization of the integral equation.

4.1 Nyström discretization

We restrict our examples in this work to integral equations along smooth boundaries Γ of genus one. As a consequence, the generating curve γ , is a smooth periodic function in \mathbb{R}^2 . The resulting integral equations along γ are discretized at equispaced points, and the resulting weakly-singular quadrature is performed using hybrid Gauss-Trapezoidal quadratures [1]. A thorough discussion of this form of discretization is contained in [22], along with a comparison with other methods. Using this discretization method, a continuous integral equation of the form

$$\sigma(s) + \int_{\gamma} K(s, s') \sigma(s') ds' = f(s), \quad \text{on } \gamma \quad (4.1)$$

is approximated by the finite dimensional system

$$\sigma_j + \frac{2\pi L}{N} \sum_{k \neq j} w_{jk} K(s_j, s_k) \sigma_k = f(s_j), \quad \text{for } j = 1, \dots, N, \quad (4.2)$$

where L is the length of γ , the w_{jk} are the quadrature weights for the Gauss-Trapezoidal rule, and σ_j is an approximation to the true solution $\sigma(s_j)$. The discretization points are given as $s_j = (j - 1)L/N$.

In the case of an iterated integral, as in our case, each operator is discretized separately and the resulting dense matrices are densely multiplied together. For example, the continuous integral equation

$$\sigma(s) + \int_{\gamma} K_2(s, s') \int_{\gamma} K_1(s', s'') \sigma(s'') ds'' ds' = f(s), \quad \text{on } \gamma \quad (4.3)$$

is approximated by the finite dimension system

$$\sigma_j + \frac{2\pi L}{N} \sum_{k \neq j} w_{jk} K_2(s_j, s_k) \frac{2\pi L}{N} \sum_{k' \neq k} w_{kk'} K_1(s_k, s_{k'}) \sigma'_{k'} = f(s_j), \quad \text{for } j = 1, \dots, N. \quad (4.4)$$

Lastly, we note that in the numerical experiments contained in Section 5 the integral equations for the generalized Debye systems are only discretized using an *odd* number of points along the generating curve. This is in order to avoid a spurious null-space issue arising from the use of trapezoidal-based discretization schemes for Cauchy or Hilbert-type integral operators, i.e. the null-space associated with the alternating-point trapezoidal rule [36]. Integral operators of this form arise in the generalized Debye formulation due to the presence of surface gradients and surface divergences. The analogous problem on fully 3D surfaces requires extra care as well [4].

We now turn to the evaluation of the modal Green's functions.

4.2 Modal Green's function evaluation

The modal separation of variables calculation for integral equations along surfaces is valid for any rotationally invariant Green's function G . Here we detail the precise calculations that are necessary when G is the Green's function for the Helmholtz equation:

$$G(\mathbf{x}, \mathbf{x}') = \frac{e^{ik|\mathbf{x}-\mathbf{x}'|}}{4\pi|\mathbf{x}-\mathbf{x}'|}. \quad (4.5)$$

Evaluation of the so-called *modal Green's functions* has received varying degrees of attention over the past several decades, ranging from brute-force integration to FFT-based methods [18, 43], as well as singularity subtraction [23], exact special function expansions [9], and contour integration [21]. While contour integration for small modes m is an attractive option due to the efficiency of the resulting schemes, constructing deformations that yield accurate results for higher modes is difficult, if not intractable. Our evaluation scheme is based on the observations in [23], with some additional numerical details filled in.

Switching to cylindrical coordinates and expanding in Fourier series,

$$G(\mathbf{x}, \mathbf{x}') = \sum_{m=-\infty}^{\infty} G_m(r, z, r', z') e^{im(\theta-\theta')}, \quad (4.6)$$

where it is obvious that for $\mathbf{x} \neq \mathbf{x}'$:

$$G_m(r, z, r', z') = \frac{1}{2\pi} \int_{-\pi}^{\pi} G(r, z, r', z', \varphi) e^{-im\varphi} d\varphi. \quad (4.7)$$

Trivially, since G is an even function, it is a function of $\cos \varphi$, and therefore $G_{-m} = G_m$. Furthermore, in fact, in the electro-/magneto-statics case when $\omega = 0$, the Fourier modes can be calculated explicitly in terms of Legendre functions of the second kind of half-order [6, 33],

$$\frac{1}{4\pi|\mathbf{x}-\mathbf{x}'|} = \frac{1}{4\pi^2\sqrt{rr'}} \sum_m Q_{m-1/2}(\chi) e^{im(\theta-\theta')}, \quad (4.8)$$

where $\chi > 1$ is given by

$$\chi = \frac{r^2 + r'^2 + (z - z')^2}{2rr'}. \quad (4.9)$$

Here we are using notation consistent with previous discussions of these functions [6, 43]. In the general $\omega \neq 0$ case, we begin by expanding the integral representation of G_m as

$$\begin{aligned} G_m(r, z, r', z') &= \frac{1}{2\pi} \int_{-\pi}^{\pi} \frac{e^{ik\sqrt{r^2+r'^2-2rr'\cos\varphi+(z-z')^2}}}{4\pi\sqrt{r^2+r'^2-2rr'\cos\varphi+(z-z')^2}} e^{-im\varphi} d\varphi \\ &= \frac{1}{8\pi^2 R_0} \int_{-\pi}^{\pi} \frac{e^{i\kappa\sqrt{1-\alpha\cos\varphi}}}{\sqrt{1-\alpha\cos\varphi}} e^{-im\varphi} d\varphi \end{aligned} \quad (4.10)$$

where the parameters κ , α , and R_0 are given by

$$\begin{aligned} \kappa &= kR_0, & \alpha &= \frac{2rr'}{R_0^2}, \\ R_0^2 &= r^2 + r'^2 + (z - z')^2, \end{aligned} \quad (4.11)$$

and we use $\varphi = \theta - \theta'$ to denote the difference in azimuthal angle. In this form, it is obvious that any numerical scheme for evaluating G_m will depend on three parameters: κ , α , and m , with α being the parameter which determines the growth of the integrand near $\varphi = 0$ ($\alpha = 1$ corresponds to the singularity in the Green's function). Based on several numerical experiments performed in quadruple precision using the Intel Fortran compiler, and the methods developed in [23, 43], the following scheme provides near machine accuracy evaluation of the sequence G_{-M}, \dots, G_M in roughly $\mathcal{O}(M \log M)$ time using the FFT:

For $0 \leq \alpha < 1/1.005 \approx .995$: These values of α correspond to sources and targets that are reasonably well-separated, and therefore the integrand in (4.10) is relatively smooth. For fixed κ , α , and R_0 , the integral in (4.10) can be discretized using the periodic trapezoidal rule and the kernels G_{-M}, \dots, G_M and their gradients can be computed using an L -point FFT, where L depends on κ and M , i.e. the frequency content of the integrand. If $|\kappa| \leq 256$, a 1024-point FFT obtains near double precision accuracy in this regime. If $|\kappa| > 256$, an L -point FFT, with $L \geq 2^{\log_2 |\kappa| + 2}$, obtains near double precision accuracy. Of course, L must be chosen large enough so that $L > 2M$ to compute G_{-M}, \dots, G_M . In practice, usually M is much smaller than L computed using the above estimates.

For $1/1.005 \leq \alpha < 1$: In this case, the source and target are relatively near to each other and the integrand in (4.10) is nearly singular. In this case, we follow the method of [23] and rewrite the integral as

$$G_m(r, z, r', z') = \frac{1}{2\pi} \int_{-\pi}^{\pi} \frac{\cos(i\kappa\sqrt{1-\alpha\cos\varphi}) + i\sin(i\kappa\sqrt{1-\alpha\cos\varphi})}{4\pi R_0\sqrt{1-\alpha\cos\varphi}} e^{-im\varphi} d\varphi.$$

Letting

$$H^c(\varphi; \kappa, \alpha) = \frac{\cos(\kappa\sqrt{1-\alpha\cos\varphi})}{\sqrt{1-\alpha\cos\varphi}}, \quad H^s(\varphi; \kappa, \alpha) = \frac{\sin(\kappa\sqrt{1-\alpha\cos\varphi})}{\kappa\sqrt{1-\alpha\cos\varphi}},$$

we now note that H^s is a very smooth function of φ , even as $\alpha \rightarrow 1$. Its Fourier modes can be computed using only a modestly sized FFT, with size at most proportional to κ .

The Fourier modes of H^c can be computed as the linear convolution of the Fourier modes of $\cos(\kappa\sqrt{1-\alpha\cos\varphi})$ and the Fourier modes of $1/\sqrt{1-\alpha\cos\varphi}$. The former modes can be computed with the FFT, and the latter functions are known analytically: they are proportional to $Q_{m-1/2}$, as in (4.8). This method for evaluating G_m was introduced in [43], and see [5] for more info on computing linear convolutions with the FFT.

We will not discuss the first case, when $0 \leq \alpha < 1/1.005$, as the numerical evaluation is as simple as applying the FFT. However, there are some details which we will highlight concerning the more difficult case, when $1/1.005 \leq \alpha < 1$. In order to compute H^c via linear convolution of $Q_{m-1/2}$ with the Fourier modes of $\cos(\kappa\sqrt{1-\alpha\cos\varphi})$, one must first evaluate the functions $Q_{m-1/2}$. The domain of relevance for these functions is $(1, \infty)$, and they exhibit log-type singularities at $\chi = 1$. These functions must be computed via backward-recurrence using Miller's algorithm, as they are the recessive solution of the pair $P_{m-1/2}, Q_{m-1/2}$ with respect to the index m [19]. Letting $\lambda = \sqrt{2}/(\chi + 1)$, the first two functions in this sequence are given explicitly in terms of elliptic integrals [33]:

$$Q_{-1/2}(\chi) = \lambda K(\lambda), \quad Q_{1/2}(\chi) = \chi \lambda K(\lambda) - \sqrt{2(\chi + 1)} E(\lambda), \quad (4.12)$$

Table 1: Sizes of forward recurrences than can be used for various values of χ to compute $Q_{m-1/2}(\chi)$ before significant loss of precision is encountered (more than 10^{-13} in absolute precision).

χ	max m
(1.0, 1.00000005]	12307
(1.00000005, 1.0000005]	4380
(1.0000005, 1.000005]	1438
(1.000005, 1.00005]	503
(1.00005, 1.0005]	163

where K and E are the complete elliptic integrals of the first- and second-kind, respectively (in the notation of [33]). Subsequent terms obey the three-term recurrence

$$Q_{m+1/2}(\chi) = 2\chi \frac{2m}{2m+1} Q_{m-1/2}(\chi) - \frac{2m-1}{2m+1} Q_{m-3/2}(\chi). \quad (4.13)$$

However, for values of $\chi \approx 1$, near the singularity, an excessive number of terms is required in order to run the forward recurrence sufficiently far in Miller's algorithm. For these values, the forward recurrence is only mildly unstable and can be used with care. Table 1 provides estimates on the number of terms that can be computed using the forward recurrence before values lose more than 2 digits in absolute precision. Using the fact that the $Q_{m-1/2}$'s form a decreasing sequence, i.e. $Q_{m+1/2} < Q_{m-1/2}$, the values in Table 1 were obtained experimentally and set to be the index m at which (numerically, in double precision) $Q_{m+1/2} > Q_{m-1/2}$. This point in the sequence indicates when loss of numerical precision begins. For values of $\chi > 1.005$, Miller's algorithm only requires only a few flops per $Q_{m-1/2}$ for nearly full double-precision.

Gradients of G_m can be computed analytically using the integral representation, and then evaluated using the previously discussed methods. Using FFTs of the same size as when evaluating G_m almost always provides commensurate accuracy. Some sophistication can be used when computed derivatives, as it involves products of several terms. It is efficient to compute Fourier modes for each term and then compute the overall convolution using the FFT. See [23, 43] for formulas regarding the gradients of G_m and $Q_{m-1/2}$.

Furthermore, the additional kernels required in the vector case, G_m^{\cos} and G_m^{\sin} , can be directly evaluated as

$$\begin{aligned} G_m^{\cos} &= \int_{-\pi}^{\pi} G(\cdot, \varphi) \cos \varphi e^{-im\varphi} d\varphi \\ &= \int_{-\pi}^{\pi} G(\cdot, \varphi) \frac{e^{i\varphi} + e^{-i\varphi}}{2} e^{-im\varphi} d\varphi \\ &= \frac{1}{2} (G_{m+1} + G_{m-1}), \\ G_m^{\sin} &= \frac{1}{2i} (G_{m+1} - G_{m-1}). \end{aligned} \quad (4.14)$$

We now describe numerical tools related to surface differentials along Γ .

4.3 Application of differentials

Using the generalized Debye source representation requires the discretization of several surface-differential operators, namely $\nabla_{\Gamma}\cdot$, ∇_{Γ} , and Δ_{Γ} . Integration by parts along Γ allow for all composition

of differential and layer-potential operators to be constructed as (at most) order-zero operators by direct differentiation on the Green's function. For example, along Γ ,

$$\begin{aligned}\mathcal{S}_0 \nabla_\Gamma \cdot \mathbf{J}(\mathbf{x}) &= \int_\Gamma G_0(\mathbf{x}, \mathbf{x}') \nabla_\Gamma \cdot \mathbf{J}(\mathbf{x}') da(\mathbf{x}') \\ &= - \int_\Gamma \nabla'_\Gamma G_0(\mathbf{x}, \mathbf{x}') \cdot \mathbf{J}(\mathbf{x}') da(\mathbf{x}'),\end{aligned}\tag{4.15}$$

where ∇'_Γ denotes the gradient with respect to the variable \mathbf{x}' . Likewise,

$$\begin{aligned}\mathcal{S}_0 \Delta_\Gamma \mathcal{S}_k \rho(\mathbf{x}) &= \mathcal{S}_0 \nabla_\Gamma \cdot \nabla_\Gamma \mathcal{S}_k \rho(\mathbf{x}) \\ &= - \int_\Gamma \nabla'_\Gamma G_0(\mathbf{x}, \mathbf{x}') \cdot \int_\Gamma \nabla'_\Gamma G_k(\mathbf{x}', \mathbf{x}'') \rho(\mathbf{x}'') da(\mathbf{x}'') da(\mathbf{x}')\end{aligned}\tag{4.16}$$

Using these identities, and the following construction of the operator $\nabla_\Gamma \Delta_\Gamma^{-1}$, it is possible to build the discretized system matrix *without* any numerical differentiation, despite the presence of so many surface differential operators.

When using the generalized Debye source representation, as described in Section 2.1, in constructing the surface vector fields \mathbf{J}, \mathbf{K} from the sources ρ, σ it is necessary to apply the inverse of the Laplace-Beltrami operator Δ_Γ . On a general surface, this is quite difficult and a topic of ongoing research [17, 25, 34]. However, on a surface of revolution, the procedure is reduced to solving a series of uncoupled ODEs. in order to evaluate $\alpha = \Delta_\Gamma^{-1} f$ we instead solve the forward problem

$$\begin{aligned}\Delta_\Gamma \alpha &= f, \\ \int_\Gamma \alpha da &= 0,\end{aligned}\tag{4.17}$$

where it is assumed that f is a mean-zero function. On a surface of revolution, this can be reduced to a sequence of uncoupled variable coefficient constrained ODEs, one for each mode m :

$$\begin{aligned}\left(\frac{\partial^2}{\partial s^2} + \frac{1}{r} \frac{\partial r}{\partial s} \frac{\partial}{\partial s} - \frac{m^2}{r^2} \right) \alpha_m &= f_m, \\ \int_\gamma \alpha_m r ds &= 0,\end{aligned}\tag{4.18}$$

where, as before,

$$\alpha(s, \theta) = \sum_m \alpha_m(s) e^{im\theta}, \quad f(s, \theta) = \sum_m f_m(s) e^{im\theta}.\tag{4.19}$$

The surface Laplacian is uniquely invertible when restricted as a map from mean-zero functions to mean-zero functions [11]. This mean-zero constraint is automatically satisfied for right-hand sides f_m with $m \neq 0$, and the ODE portion of (4.18) is invertible. For rotationally symmetric functions f_0 , the integral constraint in (4.18) must be explicitly enforced, as the ODE is not invertible. One option for solving this system is to discretize Δ_Γ pseudo-spectrally as in [25] and invert the resulting dense matrix. This procedure may suffer from ill-conditioning when γ requires many discretization points. Alternatively, letting $u = d^2 \alpha_m / ds^2$, the ODE can formally be rewritten as a second-kind integral equation with periodic boundary conditions:

$$\begin{aligned}u_m + \frac{1}{r} \frac{\partial r}{\partial s} \int u_m ds - \frac{m^2}{r^2} \iint u_m ds' ds &= f_m, \\ u_m(0) = u_m(L), \quad \frac{du_m}{ds}(0) &= \frac{du_m}{ds}(L).\end{aligned}\tag{4.20}$$

The previous integral equation can be solved for u_m by using the FFT and enforcing the proper integral constraint explicitly on u_0 [39].

Once u_m (or its Fourier series) has been computed, α_m and its first derivative can be easily and stably computed in the Fourier domain by division of the mode number and period length. Both α_m and its first derivative are needed to compute its surface gradient, as per the surface differential formulas in (3.17).

4.4 Debye auxiliary conditions

The generalized Debye formulation for scattering from genus 1 objects also involves discretizing two additional constraints on field in order to fix the projection of \mathbf{J} , \mathbf{K} onto the harmonic vector fields as per the Hodge decomposition in (2.7). Namely, to the purely azimuthal $m = 0$ mode integral equation we add in the constraints:

$$\int_{C_A} \mathbf{E}^{\text{tot}} \cdot d\mathbf{l} = 0, \quad \int_{C_B} \mathbf{E}^{\text{tot}} \cdot d\mathbf{l} = 0, \quad (4.21)$$

where the loops C_A and C_B are show in Figure 1. In the local coordinate system τ, θ, \mathbf{n} along Γ , these integrals can be rewritten as:

$$\begin{aligned} \int_{C_A} \mathbf{E} \cdot \boldsymbol{\tau} \, ds &= - \int_{C_A} \mathbf{E}^{\text{in}} \cdot \boldsymbol{\tau} \, ds, \\ \int_{C_B} \mathbf{E} \cdot \boldsymbol{\theta} \, ds &= - \int_{C_B} \mathbf{E}^{\text{in}} \cdot \boldsymbol{\theta} \, ds. \end{aligned} \quad (4.22)$$

As $\omega \rightarrow 0$, if \mathbf{E}^{in} is due to sources exterior to Ω both line integrals of \mathbf{E}^{in} are $O(\omega) \rightarrow 0$. For example, by application of Maxwell's equations and Stokes's Theorem,

$$\int_{C_A} \mathbf{E}^{\text{in}} \cdot \boldsymbol{\tau} \, ds = - \int_{S_A} i\omega\mu \mathbf{H}^{\text{in}} \cdot d\mathbf{a}, \quad (4.23)$$

where S_A is a spanning surface with boundary C_A . Furthermore, as $\omega \rightarrow 0$, the circulations of the scattered field \mathbf{E} scale as [13]:

$$\begin{aligned} \int_{C_A} \mathbf{E} \cdot \boldsymbol{\tau} \, ds &\sim O(1), \\ \int_{C_B} \mathbf{E} \cdot \boldsymbol{\theta} \, ds &\sim O(\omega). \end{aligned} \quad (4.24)$$

As a result of this scaling, difficulties arise in discretizing the circulation of \mathbf{E} along C_B as both the condition and the data tend to zero.

To overcome this scaling issue, we begin by first denoting by $\mathbf{E}(k)$ the electric field generated by the Debye sources ρ, σ and harmonic currents $\mathbf{J}_H, \mathbf{K}_H$ at wavenumber k :

$$\mathbf{E}(k) = ik\mathcal{S}_k \mathbf{J}_H - \nabla \mathcal{S}_k \rho - \nabla \times \mathcal{S}_k \mathbf{K}_H. \quad (4.25)$$

Furthermore, also note that due to (4.24),

$$\lim_{k \rightarrow 0} \int_{C_B} \mathbf{E}(k) \cdot \boldsymbol{\theta} \, ds = \int_{C_B} \mathbf{E}(0) \cdot \boldsymbol{\theta} \, ds = 0. \quad (4.26)$$

See [12] for details. Using this fact, now note that:

$$\begin{aligned}
\frac{1}{k} \int_{C_B} \mathbf{E}(k) \cdot \boldsymbol{\theta} \, ds &= \frac{1}{k} \left(\int_{C_B} \mathbf{E}(k) \cdot \boldsymbol{\theta} \, ds - \int_{C_B} \mathbf{E}(0) \cdot \boldsymbol{\theta} \, ds \right) \\
&= \int_{C_B} \left(\frac{\mathbf{E}(k) - \mathbf{E}(0)}{k} \right) \cdot \boldsymbol{\theta} \, ds \\
&= \int_{C_B} \left(\frac{\mathbf{E}(k) - \mathbf{E}(0)}{k} \right) \cdot \boldsymbol{\theta} \, ds \\
&= \int_{C_B} \mathbf{E}_{\text{diff}} \cdot \boldsymbol{\theta} \, ds,
\end{aligned} \tag{4.27}$$

where

$$\mathbf{E}_{\text{diff}} = i\mathcal{S}_k \mathbf{J} - i\nabla \times \mathcal{S}_k \left(\nabla_{\Gamma} \Delta_{\Gamma}^{-1} \rho - \mathbf{n} \times \nabla_{\Gamma} \Delta_{\Gamma}^{-1} \sigma \right) - \nabla \times \frac{1}{k} (\mathcal{S}_k - \mathcal{S}_0) \mathbf{K}_H. \tag{4.28}$$

While catastrophic cancellation (in relative precision) occurs in computing the B -cycle circulation of \mathbf{E} , the same circulation of \mathbf{E}_{diff} is $O(1)$ and can be computed stably as long as care is taken in evaluation the difference operator:

$$\mathcal{S}_{\text{diff}} = \frac{1}{k} (\mathcal{S}_k - \mathcal{S}_0). \tag{4.29}$$

For small k , expanding the numerator of the Green's function in a Taylor series about $k = 0$ and taking the first several terms achieve near machine precision. With this computation, instead of enforcing the circulation condition $\int_{C_B} \mathbf{E}^{\text{tot}} \cdot d\mathbf{l}$ we instead enforce the identical condition:

$$\begin{aligned}
\int_{C_B} \frac{\mathbf{E}(k) - \mathbf{E}(0)}{k} \cdot d\mathbf{l} &= -\frac{1}{k} \int_{C_B} \mathbf{E}^{\text{in}} \cdot d\mathbf{l} \\
&= \frac{1}{k} \int_{S_B} \nabla \times \mathbf{E}^{\text{in}} \cdot d\mathbf{a} \\
&= -i \int_{S_B} \mathbf{H}^{\text{in}} \cdot d\mathbf{a},
\end{aligned} \tag{4.30}$$

where S_B is the spanning surface for the cycle C_B .

Next, we describe the full multi-mode direct solver for computing the full electromagnetic scattering problem.

4.5 A direct solver

Using the above numerical machinery, a full system matrix discretizing each modal integral equation can be constructed. Let N denote the number of discretization points along the generating curve γ and M denote the maximum Fourier mode required in the azimuthal direction. The surface Γ is then sampled using an $N \times (2M + 1)$ tensor-product grid in $[0, L] \times [0, 2\pi]$. The fully 3D incoming fields

$$\begin{aligned}
\mathbf{E}^{\text{in}} &= E_x^{\text{in}} \mathbf{i} + E_y^{\text{in}} \mathbf{j} + E_z^{\text{in}} \mathbf{k} \\
\mathbf{H}^{\text{in}} &= H_x^{\text{in}} \mathbf{i} + H_y^{\text{in}} \mathbf{j} + H_z^{\text{in}} \mathbf{k}
\end{aligned} \tag{4.31}$$

are sampled on this grid and converted to a cylindrical coordinate vector field:

$$\begin{aligned}
\mathbf{E}^{\text{in}} &= E_r^{\text{in}} \mathbf{r} + E_{\theta}^{\text{in}} \boldsymbol{\theta} + E_z^{\text{in}} \mathbf{k} \\
\mathbf{H}^{\text{in}} &= H_r^{\text{in}} \mathbf{r} + H_{\theta}^{\text{in}} \boldsymbol{\theta} + H_z^{\text{in}} \mathbf{k}.
\end{aligned} \tag{4.32}$$

The Fourier series of each of these cylindrical components is computed via an FFT so that, for example:

$$E_r^{\text{in}} = \sum_{m=-M}^M E_{r,m}^{\text{in}} e^{im\theta}. \quad (4.33)$$

The mode-by-mode tangential projections in the local orthonormal basis are then computed as:

$$\begin{aligned} E_{\tau,m}^{\text{in}} &= \frac{dr}{ds} E_{r,m}^{\text{in}} + \frac{dz}{ds} E_{z,m}^{\text{in}}, & H_{\tau,m}^{\text{in}} &= \frac{dr}{ds} H_{r,m}^{\text{in}} + \frac{dz}{ds} H_{z,m}^{\text{in}}, \\ E_{n,m}^{\text{in}} &= \frac{dz}{ds} E_{r,m}^{\text{in}} - \frac{dr}{ds} E_{z,m}^{\text{in}}, & H_{n,m}^{\text{in}} &= \frac{dz}{ds} H_{r,m}^{\text{in}} - \frac{dr}{ds} H_{z,m}^{\text{in}}. \end{aligned} \quad (4.34)$$

For each mode $m = -M, \dots, M$, the projection of the data $\mathcal{S}_0 \nabla_\Gamma \cdot \mathbf{E}^{\text{in}}$ onto the m th Fourier mode in θ is computed as:

$$\begin{aligned} (\mathcal{S}_0 \nabla_\Gamma \cdot \mathbf{E}^{\text{in}})_m &= \left(\int_\Gamma G^0(\mathbf{x}, \mathbf{x}') \nabla_\Gamma \cdot \mathbf{E}^{\text{in}}(\mathbf{x}') da(\mathbf{x}') \right)_m \\ &= \left(- \int_\Gamma \nabla'_\Gamma G^0(\mathbf{x}, \mathbf{x}') \cdot \mathbf{E}^{\text{in}}(\mathbf{x}') da(\mathbf{x}') \right)_m \\ &= - \int_\gamma \left(\frac{dG_m^0}{ds'}(s, s') E_{t,m}^{\text{in}}(s') - \frac{im}{r} G_m^0(s, s') E_{\theta,m}^{\text{in}} \right) r ds', \end{aligned} \quad (4.35)$$

where for \mathbf{x} and \mathbf{x}' on Γ ,

$$G^0(\mathbf{x}, \mathbf{x}') = \frac{1}{4\pi|\mathbf{x} - \mathbf{x}'|}, \quad G^0(\mathbf{x}, \mathbf{x}') = \sum_m G_m^0(s, s') e^{im(\theta - \theta')}. \quad (4.36)$$

The m th Fourier mode of the data $\mathbf{n} \cdot \mathbf{H}^{\text{in}}$ is merely $H_{n,m}^{\text{in}}$. A sequence of decoupled integral equations on γ can then be solved for each m .

For the $m = 0$ mode, we solve the Nyström discretization of the system

$$\begin{aligned} \frac{1}{4} \rho_m + ik \mathcal{S}_{0,m} \nabla_{\Gamma,m} \cdot \mathcal{S}_{k,m} \mathbf{J}_m - \mathcal{S}_{0,m} \Delta_{\Gamma,m} \mathcal{S}_{k,m} \rho_m + \mathcal{S}_{0,m} \nabla_{\Gamma,m} \cdot \nabla \times \mathcal{S}_{k,m} \mathbf{K}_m &= (\mathcal{S}_0 \nabla_\Gamma \cdot \mathbf{E}^{\text{in}})_m \\ \frac{1}{2} \sigma_m + ik \mathbf{n} \cdot \mathcal{S}_{k,m} \mathbf{K}_m - \mathcal{S}'_{k,m} \sigma_m + \mathbf{n} \cdot \nabla \times \mathcal{S}_{k,m} \mathbf{J}_m &= H_{n,m}^{\text{in}} \\ \int_\gamma E_{t,m} ds &= - \int_\gamma E_{\tau,m}^{\text{in}} ds \\ 2\pi r_B \frac{E_{\theta,m}(k) - E_{\theta,m}(0)}{k} &= -i \int_{S_B} \mathbf{H}^{\text{in}} \cdot d\mathbf{a}, \end{aligned} \quad (4.37)$$

for the unknowns ρ , σ , and a_1, a_2 , the coefficients of two known harmonic vector fields along the body of revolution Γ [13], respectively:

$$\mathbf{h}_1 = \frac{1}{r} \boldsymbol{\tau}, \quad \mathbf{h}_2 = -\frac{1}{r} \boldsymbol{\theta}. \quad (4.38)$$

In (4.37), r_B denotes the radius of the B -cycle, C_B , and the subscript m denote the operator's projection on the m th Fourier mode. For differential operators this corresponds to formulae in (3.17) and for integral operators,

$$\mathcal{S}_{k,m} f(s) = 2\pi \int_\gamma G_m(s, s') f(s') r ds' \quad (4.39)$$

with G_m the Fourier modes of G in (4.5). For modes $m \neq 0$, only the first two equations in (4.37) need to be solved as the extra constraints (i.e. coefficients of the harmonic vector fields) have already been determined by the $m = 0$ mode system.

5 Numerical examples

5.1 Convergence results

Numerical results forthcoming.

5.2 Computation of radar cross section

Numerical results forthcoming.

5.3 Low-frequency behavior

Numerical results forthcoming.

5.4 High-frequency behavior

Numerical results forthcoming.

6 Conclusions

We have presented a direct solver based on the generalized Debye integral equation framework for full electromagnetic scattering from perfect electric conducting bodies which are rotationally symmetric. In particular, the scheme relies on separation of variables in the azimuthal direction and then solvers a series of smaller, uncoupled problems. The resulting generalized Debye integral equations are immune from the ill-conditioning present in other schemes due to both topological and dense-mesh breakdown as $\omega \rightarrow 0$. Furthermore, these formulations are resonance-free for all ω .

In practice, the bulk of the computation is spent evaluating modal Green's functions. The resulting code is highly parallelizable. The implementation described in this work relies on a trapezoidal-based Nyström discretization. This restricts applications to those in geometries which are reasonably well-discretized using equispaced nodes in *some* parameterization. Alternative (adaptive piecewise-polynomial) discretizations would need to be implemented for geometries whose generating curves contain complicated features or corners. The overall solver would remain the same, but details regarding quadrature and surface differentials would be different.

Extending the generalized Debye integral equations to fully 3D objects is a work in progress, and in addition to the various layer-potentials that need to be evaluated, the current formulation involves computing spanning surfaces (which is more complicated than finding loops). We are investigating other alternatives.

Acknowledgments

We would like to acknowledge Alex Barnett, Johan Helsing, and Gunnar Martinsson for many useful conversations.

References

- [1] B. Alpert. Hybrid Gauss-trapezoidal quadrature rules. *SIAM J. Sci. Comput.*, 20(5):1551–1584, 1999.
- [2] S. Ambikasaran, C. Borges, L.-M. Imbert-Gerard, and L. Greengard. Fast, adaptive, high order accurate discretization of the Lippmann-Schwinger equation in two dimensions. *SIAM J. Sci. Comput.*, 38:A1770–A1787, 2016.
- [3] A. H. Barnett and T. Betcke. Stability and convergence of the method of fundamental solutions for helmholtz problems on analytic domains. *Journal of Computational Physics*, 227(14):7003–7026, 2008.
- [4] J. Bremer and Z. Gimbutas. On the numerical evaluation of singular integrals of scattering theory. *J. Comput. Phys.*, 251:327–343, 2013.
- [5] W. L. Briggs and V. E. Henson. *The DFT: An Owner’s Manual for the Discrete Fourier Transform*. SIAM, Philadelphia, PA, 1995.
- [6] H. S. Cohl and J. E. Tohline. A compact cylindrical Green’s function expansion for the solution of potential problems. *Astrophys. J.*, 527(1):86–101, 1999.
- [7] D. Colton and R. Kress. *Integral Equation Methods in Scattering Theory*. John Wiley & Sons, Inc., 1983.
- [8] H. Contopanagos, B. Dembart, M. Epton, J. J. Ottusch, V. Rokhlin, J. L. Visher, and S. M. Wandzura. Well-conditioned boundary integral equations for three-dimensional electromagnetic scattering. *IEEE Trans. Antennas Propag.*, 50(12):1824–1830, 2002.
- [9] J. T. Conway and H. S. Cohl. Exact Fourier expansion in cylindrical coordinates for the three-dimensional Helmholtz Green function. *Z. Angew. Math. Phys.*, 61:425–442, 2010.
- [10] K. Cools, F. P. Andriulli, F. Olyslager, and E. Michielssen. Nullspaces of MFIE and Calderon Preconditioned EFIE Operators Applied to Toroidal Surfaces. *IEEE Trans. Antennas Propag.*, 57(10):3205–3215, 2009.
- [11] C. L. Epstein and L. Greengard. Debye sources and the numerical solution of the time harmonic Maxwell equations. *Commun. Pure Appl. Math.*, 63(4):413–463, 2010.
- [12] C. L. Epstein, Z. Gimbutas, L. Greengard, A. Klöckner, and M. O’Neil. A consistency condition for the vector potential in multiply-connected domains. *IEEE Trans. Magn.*, 49(3):1072–1076, 2013.
- [13] C. L. Epstein, L. Greengard, and M. O’Neil. Debye sources and the numerical solution of the time harmonic Maxwell equations II. *Commun. Pure. Appl. Math.*, 66(5):753–789, 2013.
- [14] C. L. Epstein, L. Greengard, and M. O’Neil. Debye Sources, Beltrami Fields, and a Complex Structure on Maxwell Fields. *Commun. Pure. Appl. Math.*, 68:2237–2280, 2015.
- [15] G. Fairweather and A. Karageorghis. The method of fundamental solutions for elliptic boundary value problems. *Advances in Computational Mathematics*, 9(1-2):69, 1998.

- [16] T. Frankel. *The Geometry of Physics*. Cambridge University Press, New York, NY, 2011.
- [17] M. Frittelli and I. Sgura. Virtual Element Method for the Laplace-Beltrami equation on surfaces. 2016. arXiv:1612.02369 [math.NA].
- [18] S. D. Gedney and R. Mittra. The use of the FFT for the efficient solution of the problem of electromagnetic scattering by a body of revolution. *IEEE Trans. Antennas Propag.*, 38(3):313–322, 1990.
- [19] A. Gil, J. Segura, and N. M. Temme. *Numerical Methods for Special Functions*. SIAM, Philadelphia, PA, 2007.
- [20] Z. Gimbutas and L. Greengard. Fast multi-particle scattering: A hybrid solver for the Maxwell equations in microstructured materials. *J. Comput. Phys.*, 232(1):22–32, 2013.
- [21] M. Gustafsson. Accurate and efficient evaluation of modal green’s functions. *J. Electromagnet. Wave.*, 24(10):1291–1301, 2010.
- [22] S. Hao, A. H. Barnett, P.-G. Martinsson, and P. Young. High-order accurate Nystrom discretization of integral equations with weakly singular kernels on smooth curves in the plane. *Adv. Comput. Math.*, 40:245–272, 2014.
- [23] J. Helsing and A. Karlsson. An explicit kernel-split panel-based Nyström scheme for integral equations on axially symmetric surfaces. *J. Comput. Phys.*, 272:686–703, 2014.
- [24] J. Helsing and A. Karlsson. Determination of normalized magnetic eigenfields in microwave cavities. *IEEE Transactions on Microwave Theory and Techniques*, 63(5):1457–1467, 2015.
- [25] L.-M. Imbert-Gerard and L. Greengard. Pseudo-Spectral Methods for the Laplace-Beltrami equation and the Hodge decomposition on Surfaces of Genus One. *Numer. Methods Partial. Differ. Equ.*, 33(3):941–955, 2017.
- [26] J. D. Jackson. *Classical Electrodynamics*. Wiley, New York, NY, 3rd edition, 1999.
- [27] S. Kapur and D. E. Long. IES3: Efficient Electrostatic and Electromagnetic Simulation. *Comput. Sci. & Engrg.*, pages 60–67, 1998.
- [28] A. Kirsch and P. Monk. A finite element/spectral method for approximating the time-harmonic Maxwell system in R^3 . *SIAM Journal on Applied Mathematics*, 55(5):1324–1344, 1995.
- [29] Y. Liu and A. H. Barnett. Efficient numerical solution of acoustic scattering from doubly-periodic arrays of axisymmetric objects. *Journal of Computational Physics*, 324:226–245, 2016.
- [30] J. R. Mautz and R. F. Harrington. Electromagnetic scattering from a homogeneous material body of revolution. *Archiv Elektronik und Uebertragungstechnik*, 33:71–80, 1979.
- [31] P. Monk. A finite element method for approximating the time-harmonic Maxwell equations. *Numerische Mathematik*, 63(1):243–261, 1992.
- [32] J.-C. Nedelec. *Acoustic and Electromagnetic Equations*. Springer, New York, NY, 2001.

- [33] F. W. Olver, D. W. Lozier, R. F. Boisvert, and C. W. Clark. *NIST Handbook of Mathematical Functions*. Cambridge University Press, New York, NY, USA, 1st edition, 2010. ISBN 0521140633, 9780521140638.
- [34] M. O’Neil. Second-kind integral equations for the Laplace-Beltrami problem on surfaces in three dimensions. 2017. arXiv:1705.00069 [math.NA].
- [35] C. H. Papas. *Theory of Electromagnetic Wave Propagation*. Dover, New York, NY, 1988.
- [36] A. Sidi and M. Israeli. Quadrature methods for Periodic Singular and Weakly Singular Fredholm Integral Equations. *J. Sci. Comput.*, 3(2):201–231, 1988.
- [37] J. Sifuentes, Z. Gimbutas, and L. Greengard. Randomized methods for rank-deficient linear systems. *Elec. Trans. Num. Anal.*, 44:177–188, 2015.
- [38] M. Taskinen and P. Yla-Oijala. Current and charge integral equation formulation. *IEEE Trans. Antennas Propag.*, 54(1):58–67, 2006.
- [39] L. N. Trefethen. *Spectral methods in MATLAB*. SIAM, Philadelphia, PA, 2000.
- [40] F. Vico, Z. Gimbutas, L. Greengard, and M. Ferrando-Bataller. Overcoming low-frequency breakdown of the magnetic field integral equation. *IEEE Trans. Antennas Propag.*, 61(3):1285–1290, 2013.
- [41] F. Vico, M. Ferrando, L. Greengard, and Z. Gimbutas. The Decoupled Potential Integral Equation for Time-Harmonic Electromagnetic Scattering. *Comm. Pure Appl. Math.*, 69:771–812, 2016.
- [42] K. Yee. Numerical solution of initial boundary value problems involving maxwell’s equations in isotropic media. *IEEE Trans. Antennas Propag.*, 14:302–307, 1966.
- [43] P. Young, S. Hao, and P.-G. Martinsson. A high-order Nyström discretization scheme for boundary integral equations defined on rotationally symmetric surfaces. *J. Comput. Phys.*, 231(11):4142–4159, 2012.
- [44] N. N. Youssef. Radar cross section of complex targets. *Proc. IEEE*, 77:722–734, 1989.